

Oxo Transfer Reactions Mediated by Bis(dithiolene)tungsten Analogues of the Active Sites of Molybdoenzymes in the DMSO Reductase Family: Comparative Reactivity of Tungsten and Molybdenum

Kie-Moon Sung and R. H. Holm*

Contribution from the Department of Chemistry and Chemical Biology, Harvard University, Cambridge, Massachusetts 02138

Received October 12, 2000

Abstract: The discovery of tungsten enzymes and molybdenum/tungsten isoenzymes, in which the mononuclear catalytic sites contain a metal chelated by one or two pterin–dithiolene cofactor ligands, has lent new significance to tungsten–dithiolene chemistry. Reaction of $[\text{W}(\text{CO})_2(\text{S}_2\text{C}_2\text{Me}_2)_2]$ with RO^- affords a series of square pyramidal desoxo complexes $[\text{W}^{\text{IV}}(\text{OR}')(\text{S}_2\text{C}_2\text{Me}_2)_2]^{1-}$, including $\text{R}' = \text{Ph}$ (**1**) and Pr^i (**3**). Reaction of **1** and **3** with Me_3NO gives the cis-octahedral complexes $[\text{W}^{\text{VI}}\text{O}(\text{OR}')(\text{S}_2\text{C}_2\text{Me}_2)_2]^{1-}$, including $\text{R}' = \text{Ph}$ (**6**) and Pr^i (**8**). These W(IV,VI) complexes are considered unconstrained versions of protein-bound sites of DMSOR and TMAOR (DMSOR = dimethylsulfoxide reductase, TMAOR = trimethylamine *N*-oxide reductase) members of the title enzyme family. The structure of **6** and the catalytic center of one DMSO reductase isoenzyme have similar overall stereochemistry and comparable bond lengths. The minimal oxo transfer reaction paradigm thought to apply to enzymes, $\text{W}^{\text{IV}} + \text{XO} \rightarrow \text{W}^{\text{VI}}\text{O} + \text{X}$, has been investigated. Direct oxo transfer was demonstrated by isotope transfer from $\text{Ph}_2\text{Se}^{18}\text{O}$. Complex **1** reacts cleanly and completely with various substrates XO to afford **6** and product X in second-order reactions with associative transition states. The substrate reactivity order with **1** is $\text{Me}_3\text{NO} > \text{Ph}_3\text{AsO} > \text{pyO}$ (pyridine *N*-oxide) $> \text{R}_2\text{SO} \gg \text{Ph}_3\text{PO}$. For reaction of **3** with Me_3NO , $k_2 = 0.93 \text{ M}^{-1} \text{ s}^{-1}$, and for **1** with Me_2SO , $k_2 = 3.9 \times 10^{-5} \text{ M}^{-1} \text{ s}^{-1}$; other rate constants and activation parameters are reported. These results demonstrate that bis(dithiolene)W(IV) complexes are competent to reduce both *N*-oxides and *S*-oxides; DMSORs reduce both substrate types, but TMAORs are reported to reduce only *N*-oxides. Comparison of $k_{\text{cat}}/K_{\text{M}}$ data for isoenzymes and k_2 values for isostructural analogue complexes reveals that catalytic and stoichiometric oxo transfer, respectively, from substrate to metal is faster with tungsten and from metal to substrate is faster with molybdenum. These results constitute a kinetic metal effect in direct oxo transfer reactions for analogue complexes and for isoenzymes provided the catalytic sites are isostructural. The nature of the transition state in oxo transfer reactions of analogues is tentatively considered. This research presents the first kinetics study of substrate reduction via oxo transfer mediated by bis(dithiolene)-tungsten complexes.

Introduction

As observed recently,¹ extensive advances in structure elucidation by protein crystallography and X-ray absorption spectroscopy provide a basis for the development of synthetic analogues of the active sites of molybdenum^{2–4} and tungsten^{5,6} enzymes. Accurate analogues should be incisive in revealing intrinsic structural and reactivity features. The enzyme sites contain a single metal atom bound to one or two pterin–dithiolene cofactor ligands (S_2pd) shown in Figure 1, with additional coordination provided by oxo, sulfido, hydroxo, aqua, and protein-based ligands. Under the Hille classification,² oxidized molybdoenzymes in the DMSO reductase family

include, among others, DMSO reductase (DMSOR) itself and trimethylamine *N*-oxide reductase (TMAOR). A recent reexamination of the structure of oxidized *Rhodobacter sphaeroides* (*Rs*) DMSOR at 1.3 Å resolution has demonstrated the presence of two mutually disordered sites, square pyramidal $[\text{Mo}^{\text{VI}}\text{O}_2(\text{O}\cdot\text{Ser})(\text{S}_2\text{pd})]$ and the distorted trigonal prismatic catalytic site $[\text{Mo}^{\text{VI}}\text{O}(\text{O}\cdot\text{Ser})(\text{S}_2\text{pd})_2]$, in an occupancy ratio of 0.6:0.4.⁷ This work indicates that a previous structure determination of *Rs* DMSOR was performed at a resolution (2.2 Å) insufficient to resolve the two sites.⁸ While the matter is not settled, the same behavior may apply to *Rhodobacter capsulatus* (*Rc*) DMSOR^{9,10} and *Shewanella massilia* TMAOR.¹¹ EXAFS data for *Rs*

(1) Lim, B. S.; Sung, K.-M.; Holm, R. H. *J. Am. Chem. Soc.* **2000**, *122*, 7410–7411.

(2) Hille, R. *Chem. Rev.* **1996**, *96*, 2757–2816.

(3) Romão, M. J.; Knäblein, J.; Huber, R.; Moura, J. J. G. *Prog. Biophys. Mol. Biol.* **1997**, *68*, 121–144.

(4) Kisker, C.; Schindelin, H.; Rees, D. C. *Annu. Rev. Biochem.* **1997**, *66*, 233–267.

(5) Johnson, M. K.; Rees, D. C.; Adams, M. W. W. *Chem. Rev.* **1996**, *96*, 2817–2839.

(6) Hagen, W. R.; Arendsen, A. F. *Struct. Bonding* **1998**, *90*, 161–192.

(7) Li, H.-K.; Temple, C.; Rajagopalan, K. V.; Schindelin, H. *J. Am. Chem. Soc.* **2000**, *122*, 7673–7680.

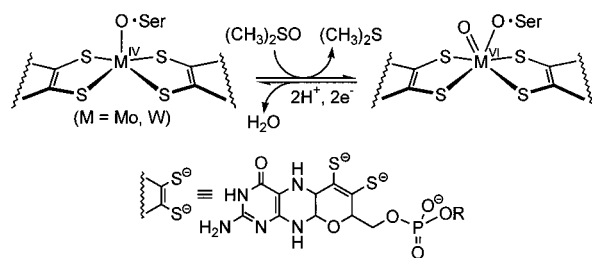
(8) Schindelin, H.; Kisker, C.; Hilton, J.; Rajagopalan, K. V.; Rees, D. C. *Science* **1996**, *272*, 1615–1621.

(9) McAlpine, A. S.; McEwan, A. G.; Shaw, A. L.; Bailey, S. *J. Biol. Inorg. Chem.* **1997**, *2*, 690–701.

(10) McAlpine, A. S.; McEwan, A. G.; Bailey, S. *J. Mol. Biol.* **1998**, *275*, 613–623.

(11) Czjzek, M.; Dos Santos, J.-P.; Pommier, J.; Giordano, G.; Méjean, V.; Haser, R. *J. Mol. Biol.* **1998**, *284*, 435–447.

Mo/W-DMSO REDUCTASE ACTIVE SITE STRUCTURE



TUNGSTEN ANALOGUE OXO TRANSFER

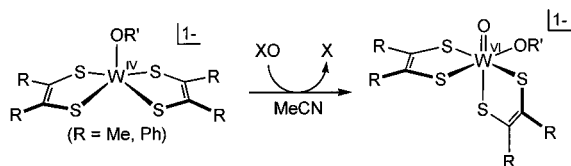


Figure 1. Proposed active site structures of reduced and oxidized Mo/W-DMSOR isoenzymes with pterin–dithiolene cofactors based on X-ray crystallography and EXAFS (top) and the oxo transfer reactions mediated by bis(dithiolene)tungsten analogue system (bottom). The structure of the pterin–dithiolene cofactor (R absent or a nucleotide) is indicated.

DMSOR¹² and *Rs* biotin sulfoxide reductase¹³ are consistent with the foregoing Mo^{VI}O site and the formulation [Mo^{IV}(O·Ser)(OH₂)(S₂pd)₂] for the dithionite-reduced enzymes.

Tungstoenzymes have been classified into two principal families: AOR (aldehyde oxidoreductases) and F(M)DH (formate dehydrogenases, FDH, and *N*-formylmethanofuran dehydrogenases, FMDH).⁵ Crystallographic information is currently limited to the structures of aldehyde¹⁴ and formaldehyde¹⁵ ferredoxin oxidoreductases from the hyperthermophilic archaeon *Pyrococcus furiosus*. The active sites contain two chelating cofactor ligands and one or two light atom, presumably oxygenous, ligands. EXAFS results for *P. furiosus* AOR are consistent with the X-ray structure.⁵ The extent to which various tungstoenzymes bind two cofactor ligands is not known.

Because of the existence of molybdenum and tungsten isoenzymes, originally detected in the F(M)DH family,^{16–18} and a more general interest in the comparative properties of these elements, we have—insofar as possible—developed the chemistry of bis(dithiolene)molybdenum and tungsten complexes in parallel.^{1,19–25,30} Since these studies were initiated, additional

(12) George, G. N.; Hilton, J.; Temple, C.; Prince, R. C.; Rajagopalan, K. V. *J. Am. Chem. Soc.* **1999**, *121*, 1256–1266.

(13) Temple, C. A.; George, G. N.; Hilton, J. C.; George, M. J.; Prince, R. C.; Barber, M. J.; Rajagopalan, K. V. *Biochemistry* **2000**, *39*, 4046–4052.

(14) Chan, M. K.; Mukund, S.; Kletzin, A.; Adams, M. W. W.; Rees, D. C. *Science* **1995**, *267*, 1463–1469.

(15) Hu, Y.; Faham, S.; Roy, R.; Adams, M. W. W.; Rees, D. C. *J. Mol. Biol.* **1999**, *286*, 899–914.

(16) (a) Schmitz, R. A.; Richter, M.; Linder, D.; Thauer, R. K. *Eur. J. Biochem.* **1992**, *207*, 559–565. (b) Bertram, P. A.; Schmitz, R. A.; Linder, D.; Thauer, R. K. *Arch. Microbiol.* **1994**, *161*, 220–228. (c) Bertram, P. A.; Karrasch, M.; Schmitz, R. A.; Böcher, R.; Albracht, S. P. J.; Thauer, R. K. *Eur. J. Biochem.* **1994**, *220*, 477–484.

(17) Schmitz, R. A.; Albracht, S. P. J.; Thauer, R. K. *Eur. J. Biochem.* **1992**, *209*, 1013–1018.

(18) Hochheimer, A.; Schmitz, R. A.; Thauer, R. K. *Eur. J. Biochem.* **1995**, *234*, 910–920.

(19) Tucci, G. C.; Donahue, J. P.; Holm, R. H. *Inorg. Chem.* **1998**, *37*, 1602–1608.

(20) Lorber, C.; Donahue, J. P.; Goddard, C. A.; Nordlander, E.; Holm, R. H. *J. Am. Chem. Soc.* **1998**, *120*, 8102–8112.

isoenzymes, highly pertinent to this investigation, have been described. These include TMAOR isoenzymes from *E. coli*; W-TMAOR also reduces sulfoxides but Mo-TMAOR does not.²⁶ The active site structures of these enzymes have not been reported. Growth of a strain of *Rc* in the presence of Na₂WO₄ results in the production of a W-DMSOR isoenzyme, whose crystal structure is very similar to that of Mo-DMSOR.²⁷ Both crystallography and tungsten EXAFS of the oxidized enzyme are consistent with the six-coordinate site formulation [W^{VI}O(O·Ser)(S₂pd)₂], but the presence of another oxygen atom, as described for the seven-coordinate oxidized Mo-DMSOR site,^{9,10} was not excluded. Molybdenum and tungsten isoenzymes are listed in Table 1 together with relative reactivities as ratios of rate constants. These results are considered in relation to kinetics data obtained in this work.

Given the structural results for *Rs* DMSOR,⁷ the operation of a direct oxo transfer pathway by this enzyme,^{28,29} and the existence of isoenzymes, we proceed on the basis of the minimal reaction paradigm M^{IV} + XO ⇌ M^{VI}O + X (M = Mo, W) in the evolution of oxo transfer analogue reactions systems.¹ Here the stoichiometric reaction or catalytic cycle operates between the desoxo M(IV) and monooxo M(VI) states as shown for DMSOR isoenzymes in Figure 1. Our initial set of bis(dithiolene) active site analogues utilized benzene-1,2-dithiolate (bdt) as a simulator of the pterin–dithiolene cofactor.^{20,21} These and dithiolene complexes derived from the ligands in Figure 1^{24,25} provide characteristic edge and EXAFS features for the identification of desoxo, monooxo, and dioxo enzyme sites.^{23,30} To afford a more realistic electronic structure and, therewith, a closer approach to the intrinsic reactivity imposed by the cofactor ligand—itsself essentially a dialkyldithiolene—we employ the ligands in Figure 1. In this investigation, we have synthesized additional bis(dithiolene)W(IV,VI) complexes for reactivity studies and investigated the kinetics and mechanism of oxo transfer in analogue reaction systems. A parallel study of oxo transfer mediated by molybdenum complexes is reported elsewhere.³¹ Certain related reactivity results for both molybdenum and tungsten systems have been communicated recently.¹ A more extensive comparison of molybdenum and tungsten oxo transfer rates is presented here.

Experimental Section

Preparation of Compounds. All operations were carried out under a pure dinitrogen atmosphere with an inert atmosphere box or standard Schlenk techniques. Solvents were distilled, dried, and degassed prior to use; ether and THF were distilled from Na/benzophenone ketyl, acetonitrile, and dichloromethane from CaH₂, and methanol from magnesium. Acetonitrile-*d*₃, dimethyl sulfoxide-*d*₆, and CD₂Cl₂ were stored over 4-Å molecular sieves for at least 1 d. Lithium 2-adaman-

(21) Donahue, J. P.; Goldsmith, C. R.; Nadiminti, U.; Holm, R. H. *J. Am. Chem. Soc.* **1998**, *120*, 12869–12881.

(22) Goddard, C. A.; Holm, R. H. *Inorg. Chem.* **1999**, *38*, 5389–5398.

(23) Musgrave, K. B.; Donahue, J. P.; Lorber, C.; Holm, R. H.; Hedman, B.; Hodgson, K. O. *J. Am. Chem. Soc.* **1999**, *121*, 10297–10307.

(24) Lim, B. S.; Donahue, J. P.; Holm, R. H. *Inorg. Chem.* **2000**, *39*, 263–273.

(25) Sung, K.-M.; Holm, R. H. *Inorg. Chem.* **2000**, *39*, 1275–1281.

(26) Buc, J.; Santini, C.-L.; Giordani, R.; Czjzek, M.; Wu, L.-F.; Giordano, G. *Mol. Microbiol.* **1999**, *32*, 159–168.

(27) Stewart, L. J.; Bailey, S.; Bennett, B.; Charnock, J. M.; Garner, C. D.; McAlpine, A. S. *J. Mol. Biol.* **2000**, *299*, 593–600.

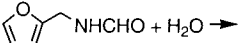
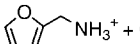
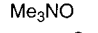
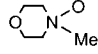
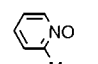
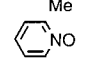
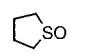
(28) Schultz, B. E.; Holm, R. H.; Hille, R. *J. Am. Chem. Soc.* **1995**, *117*, 827–828.

(29) Garton, S. D.; Hilton, J.; Oku, H.; Crouse, B. R.; Rajagopalan, K. V.; Johnson, M. K. *J. Am. Chem. Soc.* **1997**, *119*, 12906–12916.

(30) Musgrave, K. B.; Lim, B. S.; Sung, K.-M.; Holm, R. H.; Hedman, B.; Hodgson, K. O. *Inorg. Chem.* **2000**, *39*, 5238–5247.

(31) Lim, B. S.; Holm, R. H. *J. Am. Chem. Soc.* **2001**, *123*, 1920–1930.

Table 1. Relative Reactivities of Molybdenum and Tungsten Isoenzymes

isoenzyme	organism	reaction	W/Mo reactivity ratio	ref
FMDH (<i>N</i> -formylmethanofuran dehydrogenase)	<i>Methanobacterium thermoautotrophicum</i>	 + H ₂ O →	0.2	16
	<i>Methanobacterium wolfei</i>	 + NH ₃ ⁺ + CO ₂ + H ⁺ + 2e ⁻	0.3	
TMAOR (trimethylamine <i>N</i> -oxide reductase)	<i>Escherichia coli</i>	XO + 2H ⁺ + 2e ⁻ → X + H ₂ O	XO	
				2.2
				4.1
				4.2
				2.0
			Me ₂ SO	no reaction for Mo $k_{\text{cat}}/K_{\text{M}} = 5.0 \times 10^4 \text{ M}^{-1} \text{ s}^{-1}$ for W
			Ph ₂ SO	no reaction for Mo $k_{\text{cat}}/K_{\text{M}} = 2.7 \times 10^4 \text{ M}^{-1} \text{ s}^{-1}$ for W
	no reaction for Mo $k_{\text{cat}}/K_{\text{M}} = 2.0 \times 10^6 \text{ M}^{-1} \text{ s}^{-1}$ for W			
DMSOR (dimethylsulfoxide reductase)	<i>Rhodobacter capsulatus</i>	Me ₂ SO + 2H ⁺ + 2e ⁻ ⇌ Me ₂ S + H ₂ O	17 (forward reaction) 0.06 (backward reaction)	27

tyloxide was prepared by the lithiation of 2-adamantanol at -78 °C with BuⁿLi in THF. The compounds NaOC₆H₄-*p*-X (X = CN, Br, Me, OMe, NH₂) were prepared from the reaction of NaOMe with *p*-XC₆H₄-OH (purified by sublimation) in methanol. Trimethylamine *N*-oxide, pyridine *N*-oxide, and 4-methylmorpholine *N*-oxide were sublimed under reduced pressure. The compound Ph₂Se¹⁸O (62% ¹⁸O-enriched) was synthesized by a reported method.²⁰ Dimethyl sulfoxide (Aldrich, 99%) was dried over 4-Å molecular sieves and tetramethylene sulfoxide (Aldrich, 96%) was dried over CaH₂ and distilled under 0.3 Torr at 100 °C. Other compounds were of commercial origin and used as received. Solvent removal and drying steps were performed in vacuo. Filtrations were through Celite; compounds were isolated by filtration unless otherwise stated.

(Et₄N)[W(OPh)(S₂C₂Ph₂)₂]. To a dark purple solution of 107 mg (0.15 mmol) of [W(CO)₂(S₂C₂Ph₂)₂]²² in 1.5 mL of THF was added 18.1 mg (0.16 mmol) of solid NaOPh. A green-brown solution developed within 5 min and was stirred for 1 h. This solution was treated with 26.9 mg (0.16 mmol) of Et₄NCl in 1 mL of acetonitrile and the solvents were removed. The resulting brown solid was redissolved in 2 mL of acetonitrile and the solution was filtered. Ether (60 mL) was layered on the filtrate, producing 45.5 mg (34%) of green-brown crystalline solid over 1 d, which was isolated, washed with ether (3 × 1 mL), and dried. ¹H NMR (CD₃CN, anion): δ 6.6–7.4 (m). Absorption spectrum (acetonitrile): λ_{max} (ε_M) 310 (26 000), 380 (sh, 6700), 500 (sh, 1800), 680 (980) nm. Anal. Calcd for C₄₂H₄₅NOS₄W: C, 56.56; H, 5.09; N, 1.57; S, 14.38. Found: C, 56.42; H, 5.15; N, 1.47; S, 14.30.

(Et₄N)[W(OPr^f)(S₂C₂Me₂)₂]. To a solution of 205 mg (0.43 mmol) of [W(CO)₂(S₂C₂Me₂)₂]²² in 2 mL of THF was added 37.1 mg (0.45 mmol) of solid NaOPr^f. The solution turned from dark violet to brown immediately. The reaction mixture was stirred for 10 min and treated with 74.7 mg (0.45 mmol) of Et₄NCl in 1 mL of acetonitrile, and the solvents were removed. The resulting brown solid was redissolved in 1.5 mL of acetonitrile and the solution was filtered. Ether (50 mL) was layered on the brown filtrate affording 132 mg (50%) of brown microcrystalline solid over 1 d, which was isolated, washed with ether (3 × 1 mL), and dried. ¹H NMR (CD₃CN, anion): δ 0.84 (d, 6, *J* = 6.0 Hz), 2.52 (s, 12), 3.75 (heptet, 1, *J* = 6.4 Hz). Absorption spectrum

(acetonitrile): λ_{max} (ε_M) 284 (10 000), 309 (8500), 340 (sh, 3900), 380 (sh, 1400), 423 (850), 545 (270), 670 (120) nm. Anal. Calcd for C₁₉H₃₉NOS₄W: C, 37.43; H, 6.45; N, 2.30; S, 21.04. Found: C, 37.54; H, 6.38; N, 2.30; S, 21.12.

(Et₄N)[W(2-AdO)(S₂C₂Me₂)₂]. To a suspension of 21.3 mg (0.13 mmol) of 2-AdOLi (Ad = adamantyl) in 0.5 mL of acetonitrile was added a violet solution of 64.5 mg (0.14 mmol) of [W(CO)₂(S₂C₂Me₂)₂] in 2 mL of THF. A red-brown color developed immediately; the reaction mixture was stirred for 30 min. After the treatment with 22.2 mg (0.13 mmol) of Et₄NCl, the solvents were removed. The resulting brown solid was redissolved in 1.5 mL of acetonitrile and the solution was filtered. Onto the brown filtrate was layered 10 mL of ether. Over 6 h, needlelike crystals deposited. These were isolated, washed with ether (3 × 1 mL), and dried to afford 50.5 mg (53%) of dark brown crystals. ¹H NMR (CD₃CN, anion): δ 1.41–1.66 (m, 14), 2.50 (s, 12), 3.49 (s, 1). Absorption spectrum (acetonitrile): λ_{max} (ε_M) 283 (11 000), 307 (9100), 340 (sh, 4500), 380 (sh, 1700), 423 (920), 544 (300), 670 (110) nm. Anal. Calcd for C₂₆H₄₇NOS₄W: C, 44.50; H, 6.75; N, 2.00; S, 18.28. Found: C, 44.68; H, 6.71; N, 1.98; S, 18.37.

(Et₄N)[W(O-*p*-C₆H₄X)(S₂C₂Me₂)₂]. These compounds were prepared on a 0.10–0.22 mmol scale by a procedure analogous to that for (Et₄N)[W(OPh)(S₂C₂Me₂)₂]²⁵ with NaOC₆H₄-*p*-X instead of NaOPh.

X = CN: Dark brown block-shaped crystals. Yield: 35%. IR (KBr): ν(CN) 2221(m) cm⁻¹. ¹H NMR (CD₃CN, anion): δ 2.62 (s, 12), 6.56 (d, 2, *J* = 8.8 Hz), 7.38 (d, 2, *J* = 8.8 Hz). Absorption spectrum (acetonitrile): λ_{max} (ε_M) 282 (21 000), 330 (sh, 11 000), 360 (sh, 3900), 408 (3000), 490 (820) 660 (320) nm. Anal. Calcd for C₂₃H₃₆N₂OS₄W: C, 41.31; H, 5.43; N, 4.19; S, 19.18. Found: C, 41.39; H, 5.40; N, 4.08; S, 19.29.

X = Br: Dark brown block-shaped crystals. Yield: 46%. ¹H NMR (CD₃CN, anion): δ 2.62 (s, 12), 6.33 (d, 2, *J* = 8.8 Hz), 7.21 (d, 2, *J* = 8.8 Hz). Absorption spectrum (acetonitrile): λ_{max} (ε_M) 291 (15 000), 319 (sh, 12 000), 347 (sh, 4800), 398 (2700), 478 (760) 658 (380) nm. Anal. Calcd for C₂₂H₃₆NOBrS₄W: C, 36.57; H, 5.02; N, 1.94; Br, 11.06; S, 17.75. Found: C, 36.47; H, 5.10; N, 1.86; Br, 10.98; S, 17.87.

X = Me: Brown needle-shaped crystals. Yield: 60%. ¹H NMR (CD₃CN, anion): δ 2.12 (s, 3), 2.60 (s, 12), 6.30 (d, 2, *J* = 8.4 Hz), 6.80 (d, 2, *J* = 8.4 Hz). Absorption spectrum (acetonitrile): λ_{max} (ε_M)

Chart 1. Abbreviations and Designation of Tungsten Complexes

$[\text{W}^{\text{IV}}(\text{OPh})(\text{S}_2\text{C}_2\text{Me}_2)_2]^{1-}$	1 ^{25,30}
$[\text{W}^{\text{IV}}(\text{OPh})(\text{S}_2\text{C}_2\text{Ph}_2)_2]^{1-}$	2
$[\text{W}^{\text{IV}}(\text{OPr}^f)(\text{S}_2\text{C}_2\text{Me}_2)_2]^{1-}$	3
$[\text{W}^{\text{IV}}(2\text{-AdO})(\text{S}_2\text{C}_2\text{Me}_2)_2]^{1-}$	4 ³⁰
$[\text{W}^{\text{IV}}(\text{O-}i>p\text{-C}_6\text{H}_4\text{X})(\text{S}_2\text{C}_2\text{Me}_2)_2]^{1-}$	5
(X = CN, 5a ; Br, 5b ; Me, 5c ; OMe, 5d ; NH ₂ , 5e)	
$[\text{W}^{\text{VI}}\text{O}(\text{OPh})(\text{S}_2\text{C}_2\text{Me}_2)_2]^{1-}$	6 ^{1,30}
$[\text{W}^{\text{VI}}\text{O}(\text{OPh})(\text{S}_2\text{C}_2\text{Ph}_2)_2]^{1-}$	7
$[\text{W}^{\text{VI}}\text{O}(\text{OPr}^f)(\text{S}_2\text{C}_2\text{Me}_2)_2]^{1-}$	8
$[\text{W}^{\text{VI}}\text{O}(2\text{-AdO})(\text{S}_2\text{C}_2\text{Me}_2)_2]^{1-}$	9
$[\text{W}^{\text{VI}}\text{O}(\text{O-}i>p\text{-C}_6\text{H}_4\text{X})(\text{S}_2\text{C}_2\text{Me}_2)_2]^{1-}$	10
(X = CN, 10a ; Br, 10b ; Me, 10c ; OMe, 10d ; NH ₂ , 10e)	
$[\text{W}^{\text{IV}}\text{O}(\text{S}_2\text{C}_2\text{Me}_2)_2]^{2-}$	11 ²²

2-Ad	2-adamantyl
AOR	aldehyde oxidoreductase
bdt	benzene-1,2-dithiolate(2-)
Bu ^t -NS	bis(4- <i>tert</i> -butylphenyl)-2-pyridylmethanethiolate(1-)
DMSOR	dimethylsulfoxide reductase
F(M)DH	formate (<i>N</i> -formylmethanofuran) dehydrogenase
mnt	maleonitriledithiolate(2-)
NMMO	<i>N</i> -methylmorpholine <i>N</i> -oxide
<i>Pf</i>	<i>Pyrococcus furiosus</i>
pyO	pyridine <i>N</i> -oxide
<i>Rc</i>	<i>Rhodobacter capsulatus</i>
<i>Rs</i>	<i>Rhodobacter sphaeroides</i>
S ₂ pd	pterin-dithiolene cofactor ligand
TMAOR	trimethylamine <i>N</i> -oxide reductase
TMS	tetramethylenesulfide
TMSO	tetramethylenesulfoxide

295 (14 000), 319 (sh, 10 000), 347 (sh, 4000), 393 (2000), 478 (520), 580 (200) nm. Anal. Calcd for C₂₃H₃₉NOS₄W: C, 42.00; H, 5.98; N, 2.13; S, 19.50. Found: C, 42.68; H, 6.10; N, 1.95; S, 19.41.

X = OMe: Brown needle-shaped crystals. Yield: 53%. ¹H NMR (CD₃CN, anion): δ 2.60 (s, 12), 3.62 (s, 3), 6.34 (d, 2, *J* = 8.8 Hz), 6.55 (d, 2, *J* = 8.8 Hz). Absorption spectrum (acetonitrile): λ_{max} (ε_M) 295 (16 000), 319 (sh, 11 000), 347 (sh, 4100), 390 (2000), 478 (550), 569 (250). Anal. Calcd for C₂₃H₃₉NO₂S₄W: C, 41.01; H, 5.84; N, 2.08; S, 19.04. Found: C, 41.05; H, 5.92; N, 2.05; S, 19.13.

X = NH₂: Green-brown block-shaped crystals. Yield: 49%. IR (KBr): ν(NH₂) 3327 (m), 3397 (m) cm⁻¹. ¹H NMR (CD₃CN, anion): δ 2.09 (s, 2), 2.59 (s, 12), 6.18 (d, 2, *J* = 8.8 Hz), 6.27 (d, 2, *J* = 8.8 Hz). Absorption spectrum (acetonitrile): λ_{max} (ε_M) 297 (18 000), 316 (sh, 16 000), 394 (sh, 2500), 478 (sh, 720), 572 (310) nm. Anal. Calcd for C₂₂H₃₈N₂OS₄W: C, 40.12; H, 5.82; N, 4.25; S, 19.47. Found: C, 40.16; H, 6.02; N, 4.33; S, 19.55.

(Et₄N)[WO(OPh)(S₂C₂Me₂)₂]. To a frozen solution of 83.4 mg (0.13 mmol) of (Et₄N)[W(OPh)(S₂C₂Me₂)₂]²⁵ in ca. 4 mL of acetonitrile in a dry ice-acetone bath was injected a solution of 15.0 mg (0.20 mmol) of Me₃NO in 0.15 mL of MeCN. The frozen mixture was gradually warmed to -15 °C over 30 min, resulting in a color change to dark violet from green-brown. This solution was treated with 50 mL of cold ether (-15 °C) and maintained at -20 °C over 1 d during which black needlelike crystals separated. The solid was isolated by decantation of the pale brown supernatant, washed with 10 mL of cold ether (-15 °C), and dried to give the product as 65.1 mg (76%) of black crystals.

IR (KBr): ν(WO) 895 cm⁻¹. ¹H NMR (CD₃CN, anion): δ 2.19 (s, 12), 6.79 (t, 1, *J* = 7.2 Hz), 6.94 (d, 2, *J* = 7.0 Hz), 7.18 (t, 2, *J* = 8.8 Hz). Absorption spectrum (acetonitrile): λ_{max} (ε_M) 299 (sh, 11 000), 337 (8000), 408 (sh, 5000), 514 (5000), 637 (2500) nm. Anal. Calcd for C₂₂H₃₇NO₂S₄W: C, 40.06; H, 5.65; N, 2.12; S, 19.44. Found: C, 40.14; H, 5.61; N, 2.06; S, 19.51.

(Et₄N)[WO(OPr^f)(S₂C₂Me₂)₂]. To a brown solution of 37.2 mg (0.061 mmol) of (Et₄N)[W(OPr^f)(S₂C₂Me₂)₂] in 2 mL of acetonitrile was added 6.87 mg (0.091 mmol) of Me₃NO in 0.2 mL of acetonitrile at room temperature. The solution color changed to green-brown over 1 min; the solution was stirred for 10 min and 30 mL of ether was added. A black crystalline solid deposited over 2 d, which was isolated by decantation of the pale green-brown supernatant, washed with ether (3 × 1 mL), and dried to give 11.3 mg (30%) of brown-black crystalline solid. IR (KBr): ν(WO) 885 cm⁻¹. ¹H NMR spectrum (CD₃CN, anion): δ 1.06 (d, 6, *J* = 5.6 Hz), 2.13 (s, 12), 4.74 (heptet, 1, *J* = 5.6 Hz). Absorption spectrum (acetonitrile): λ_{max} (ε_M) 331 (4400), 410 (2200), 487 (3000), 632 (1800) nm. Anal. Calcd for C₁₉H₃₉NO₂S₄W: C, 36.48; H, 6.28; N, 2.24; S, 20.50. Found: C, 36.40; H, 6.35; N, 2.40; S, 20.56.

¹⁸O Transfer Reactions. To a solution of (Et₄N)[W(OPh)(S₂C₂Me₂)₂] (6.3 mg, 9.8 μmol) in 0.5 mL of acetonitrile was added a solution of Ph₂Se¹⁸O (3.2 mg, 13 μmol) in 0.5 mL of acetonitrile. This mixture was shaken for 3 min. The solvent was removed and the residue was dried in vacuo. IR (KBr): 895 (W¹⁶O), 848 (W¹⁸O) cm⁻¹.

In the sections that follow, tungsten complexes are referred to by the numerical designations in Chart 1, which also includes abbreviations used.

X-ray Structure Determinations. The structures of the five compounds in Table 2 were determined. Single crystals were obtained by layering ether onto acetonitrile solutions at ambient temperature ((Et₄N)[**2,3,4,5e**]) or at -15 °C ((Et₄N)[**6**]). Selected crystals were coated in silicone grease and mounted on a Siemens (Bruker) SMART CCD diffractometer equipped with an LT-2 low-temperature apparatus operating at 213 K. Mo Kα radiation (λ = 0.71073 Å) was used for data collection. Data were collected with ω scans of 0.3°/frame for 30 s, such that 1271 frames were collected for a hemisphere of data. The first 50 frames were recollected at the end of the data collection to monitor for decay; no significant decay was detected for any compounds. Data only out to 2θ of 50° for (Et₄N)[**2**] were used because of the low-quality high-angle data while data out to 2θ of 56.4–56.6° were employed for the other compounds. Cell parameters were retrieved by using SMART software and refined by using SAINT software on all reflections. Data reduction was performed with the SAINT software, which corrects for Lorentz polarization and decay. Absorption corrections were applied with SADABS. The space groups for all compounds were assigned unambiguously by analysis of symmetry and systematic absences determined by the program XPREP. Missing symmetry was checked by the program PLATON; no significant missing symmetry was observed. Crystal parameters are given in Table 2.

Structures were solved by direct methods with SHELXS-97 and subsequently refined against all data by full-matrix least squares on *F*² with SHELXL-97. Asymmetric units contain one-half ((Et₄N)[**4**]), one ((Et₄N)[**5e,6**]), and two ((Et₄N)[**2,3**]) formula weights; equivalent atoms were generated by symmetry transformations for (Et₄N)[**4**]. In (Et₄N)-[**4**], atoms C5, C7, and C11 of the adamantyl group are severely disordered over two positions and were refined with a site occupancy factor of 0.5; adamantyl carbon atoms were refined isotropically. All methylene groups of the cations in (Et₄N)[**4,5e,6**] are highly disordered over two positions and were refined with a site occupancy factor of 0.5. All non-hydrogen atoms including those of the disordered cations were refined anisotropically. In the final refinement, hydrogen atoms were attached at idealized positions on carbon atoms. Selected bond distances and angles are listed in Table 3. (See the paragraph at the end of the article for Supporting Information available.)

The structure of (Et₄N)[**8**] was also investigated. This compound crystallizes in monoclinic space group *P2₁/n* with *a* = 9.176(1) Å, *b* = 17.641(1) Å, *c* = 16.139(1) Å, β = 98.126(1)°, *V* = 2586.1(4) Å³, and *Z* = 4. Because of disorder, an accurate structure was not obtained. However, the overall structure of the anion is the same as that of **6**.

Table 2. Crystallographic Data^a

	(Et ₄ N)[2]	(Et ₄ N)[3]	(Et ₄ N)[4]	(Et ₄ N)[5e]	(Et ₄ N)[6]
formula	C ₄₂ H ₄₅ NOS ₄ W	C ₁₉ H ₃₉ NOS ₄ W	C ₂₆ H ₄₇ NOS ₄ W	C ₂₂ H ₃₈ N ₂ O ₅ W	C ₂₂ H ₃₇ NO ₂ S ₄ W
fw	891.88	609.60	701.74	658.63	659.62
crystal system	monoclinic	monoclinic	orthorhombic	monoclinic	monoclinic
space group	P2 ₁ /c	P2 ₁ /n	Pnma	P2 ₁ /c	P2 ₁ /c
Z	8	8	4	4	4
a, Å	15.109(3)	9.1267(5)	23.918(1)	18.149(2)	10.0883(4)
b, Å	19.512(7)	39.135(2)	11.4484(5)	8.8873(12)	15.8029(6)
c, Å	28.167(6)	14.2182(7)	11.1165(5)	18.151(2)	16.8607(6)
β, deg	102.537(18)	95.647(1)		114.667(7)	98.602(1)
V, Å ³	8105(4)	5053.7(5)	3044.0(2)	2660.6(5)	2657.77(17)
d _{calc} , g/cm ³	1.462	1.602	1.531	1.664	1.648
2θ range, deg	2.6–50	2.1–56.6	3.4–56.4	2.5–56.6	3.6–56.5
GOF (F ²)	1.082	1.007	1.038	1.018	1.059
R ₁ ^b (wR ₂ ^c)	0.0614 (0.1129)	0.0417 (0.0796)	0.0366 (0.0922)	0.0277 (0.0626)	0.0361 (0.0661)

^a Obtained with graphite-monochromatized Mo Kα (λ = 0.71073 Å) radiation at 213 K. ^b R₁ = Σ||F_o| - |F_c||/Σ|F_o|. ^c wR₂ = {Σ[w(F_o² - F_c²)]/Σ[w(F_o²)]^{1/2}.

Table 3. Selected Bond Distances (Å) and Angles (deg)

	2 ^a	3 ^a	4 ^b	5e	6
W=O ^c					1.728(3)
W-O ^d	1.827(8)	1.840(4)	1.826(4)	1.868(2)	1.994(4)
W-S1	2.309(3)	2.322(2)	2.327(1)	2.332(1)	2.492(1) ^e
W-S2	2.318(3)	2.319(2)	2.336(1)	2.326(1)	2.432(1)
W-S3	2.320(3)	2.338(2)		2.307(1)	2.402(1)
W-S4	2.317(3)	2.343(2)		2.320(1)	2.413(1)
S-C ^f	1.79(1)	1.776(5)	1.771(3)	1.781(9)	1.74(2)
C-C ^{f,g}	1.338	1.330	1.333	1.311	1.336
O-W-O					93.3(2)
O-W-S ^h					146.0(1)
W-O-C ^d	145.0(8)	141.9(4)	119.3(8) ⁱ	141.3(2)	141.0(3)
S1-W-S2 ^j	82.7(1)	82.66(6)	82.79(6) ^k	82.04(4)	77.26(5)
S3-W-S4 ^j	82.7(1)	82.56(6)	81.86(6) ^j	82.38(3)	79.13(5)
S1-W-S4 ^m	142.6(1)	144.59(6)	142.78(4) ⁿ	144.64(4)	96.00(5)
S2-W-S3 ^m	140.8(1)	139.24(6)		136.47(4)	153.49(5)
δ ^o	0.756	0.760	0.744	0.782	
θ _d ^p	128.2	128.4	129.8	126.5	99.8

^a One of two anions in the asymmetric unit; both have very similar metric parameters. ^b Symmetry transformations used to generate equivalent atoms: x, -y + 1/2, z. ^c Terminal oxo ligand. ^d Unidentate ligand. ^e Trans to oxo. ^f Mean value. ^g Chelate ring. ^h O1-W-S1. ⁱ One of the disordered carbon atoms considered. ^j Chelate ring bite angle. ^k S1-W-S1A. ^l S2-W-S2A. ^m Transoid angle. ⁿ S1-W-S2A and S1A-W-S2 are identical. ^o Perpendicular displacement of W atom from S₄ least-squares plane. ^p Dihedral angle between WS₂ planes.

Kinetics Measurements. Reactions were performed under anaerobic conditions in acetonitrile solutions, and were monitored with a Varian Cary 3 spectrophotometer equipped with a cell compartment thermostated to ±0.5 °C and a multicell changer. Thermal equilibrium was reached by placing a quartz cell (1 mm path length) containing 0.3 mL of a W(IV) compound solution into the cell compartment at least 5 min prior to reaction initiation. Reactions were initiated by the injection of substrate (or its solution) through the rubber septum cap of the quartz cell using a gastight syringe (50 μL) followed by rapid shaking of the reaction mixture.

Reductions of *N*-oxide and *S*-oxide substrates by W(IV) complexes **1–3** and **5a–e** and hydrolysis of **1** and **3** were monitored spectrophotometrically in the region 280–700 nm. Sharp isosbestic points were observed for all reaction systems. Reactions were run under pseudo-first-order conditions for the reduction of relatively weak oxo donors such as pyO, *S*-oxides, and Ph₃AsO, and for hydrolysis. Initial W(IV) complex concentrations [W^{IV}]₀ = 0.45–1.2 mM; oxo donor substrates were present at [XO]₀ = 150–4000 equiv (DMSO, TMSO), 7–40 equiv (pyO, Ph₃AsO), ca. 7500 equiv (neat TMSO), and 1000–20000 equiv (H₂O, D₂O). For faster reactions, mixed-second-order conditions were applied with [W^{IV}]₀ = 0.97–1.4 mM and 2–3 equiv of *N*-oxide. Reactions were conducted at five or six temperatures in the range of 290–333 K. At each temperature, at least five independent runs with different initial concentrations [XO]₀ were performed in the case of pseudo-first-order conditions. Plots of ln[(A_t - A_∞)/(A₀ - A_∞)] vs time

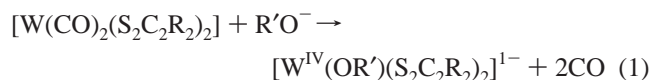
were linear over at least 3 half-lives and the initial rate constants *k*_{obs} were obtained from the plots by using data for the first 30 min. Plots of *k*_{obs} vs [XO]₀ were linear and yielded overall second-order rate constants *k*₂ at each temperature. In the case of mixed-second-order conditions,³² the second-order rate constants were obtained from the plots of {ln{[XO]_t/[W^{IV}]_t} - ln{[XO]₀/[W^{IV}]₀}/([XO]₀ - [W^{IV}]₀) vs time, where the values of [W]_t and [XO]_t were calculated from the equations of [W^{IV}]_t = [W^{IV}]₀ - (A_t - A₀)/(A_∞ - A₀) × [W^{IV}]₀ and [XO]_t = [XO]₀ - (A_t - A₀)/(A_∞ - A₀) × [W^{IV}]₀, respectively. In mixed-second-order kinetics, *k*₂ was averaged from the values that were obtained from multiple independent runs to minimize experimental errors. For the hydrolysis of **1** and **3**, Michaelis–Menten kinetics were applied and plots of 1/*k*_{obs} vs 1/[H₂O or D₂O] were linear to yield *k*₂[′] and *K*_M. Activation parameters were determined from plots of the Eyring equation *k* = (*k*_B*T*/h)[exp(Δ*S*[‡]/*R* - Δ*H*[‡]/*RT*)]. Standard deviations for rate constants were estimated by using linear least-squares error analysis, with uniform weighting of the data points.³³

Other Physical Measurements. All measurements were performed under anaerobic conditions. Absorption spectra were recorded with a Varian Cary 50 Bio or a Cary 3 spectrophotometer. ¹H NMR spectra were obtained with Varian Mercury 400/500 spectrometers. IR spectra were measured with KBr pellets with a Nicolet Nexus 470 FT-IR instrument.

Results and Discussion

In this investigation, we seek W(IV,VI) complexes that serve as analogues of the sites of tungsten isoenzymes of the DMSOR family of molybdoenzymes. Consequently, we require syntheses of desoxo and monooxo complexes [W^{IV}(OR′)(S₂C₂R₂)₂]¹⁻ and [W^{VI}O(OR′)(S₂C₂R₂)₂]¹⁻, respectively, of which only two examples (**1**²⁵ and **6**¹) have been reported earlier. Synthetic methods are outlined in Figure 2. All complexes were isolated as crystalline Et₄N⁺ salts.

Synthesis and Structures of W(IV) Complexes. These complexes are readily prepared by carbonyl displacement reaction 1 (R = Me, Ph), which affords products with aryloxo (**1**, **2**, **5**) and alkoxo (**3**, **4**) terminal ligands in yields of ca.



35–70%. The set **5a–e** was prepared to ascertain the effect of para-substituent X on substrate reduction rates. In solution, the W(IV) complexes are highly sensitive to trace amounts of water

(32) Espenson, J. H. *Chemical Kinetics and Reaction Mechanisms*; McGraw-Hill: New York, 1995.

(33) Clifford, A. A. *Multivariate Error Analysis*; Halsted Press: New York, 1973.

SYNTHESIS OF BIS(DITHIOLENE)W(IV/VI) COMPLEXES

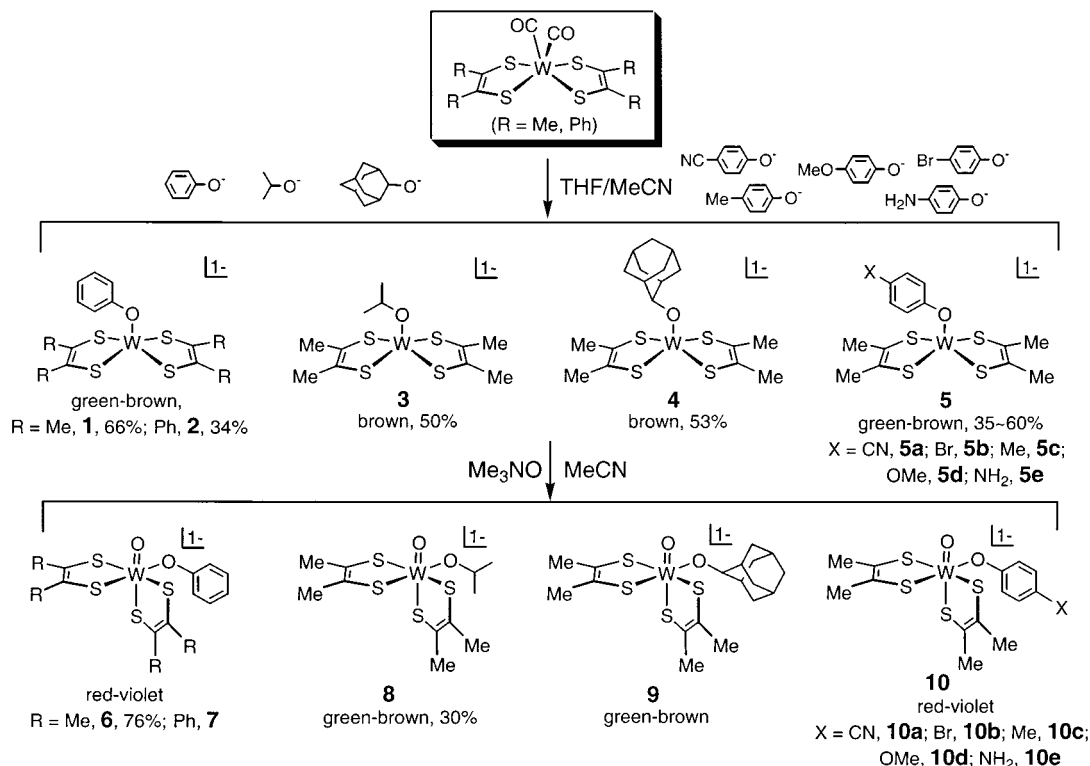


Figure 2. Synthesis of desoxo bis(dithiolene)W(IV) (1–5) and monooxo W(VI) (6–10) complexes. Complexes 7, 9, and 10 were generated in solution but not isolated.

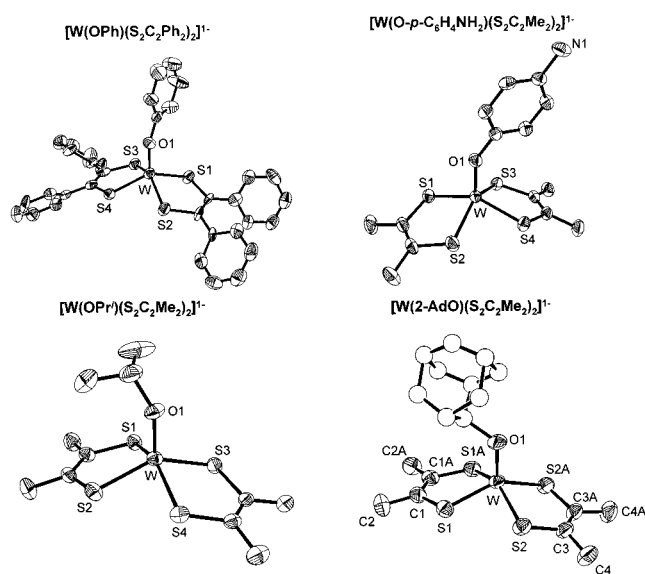
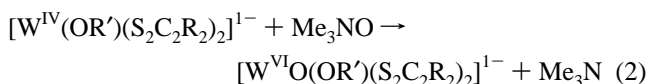


Figure 3. Structures of desoxo complexes 2–4 and 5e showing 50% probability ellipsoids and partial atom labeling schemes. The disordered carbon atoms of the adamantyl group in 4 were refined isotropically, and to dioxygen, which causes rapid oxidation to blue $[\text{W}^{\text{VI}}\text{O}(\text{S}_2\text{C}_2\text{R}_2)_2]^{1-}$.²²

The structures of four desoxo W(IV) complexes are set out in Figure 3; metric parameters are summarized in Table 3. These complexes adopt a square pyramidal structure in which the tungsten atoms are 0.74–0.78 Å above the S₄ mean plane formed by planar dithiolene ligands disposed at dihedral angles of 126–130°. The bond distances W–OR' are little affected by R' and fall into the range 1.826(4)–1.868(2) Å. The bond angles W–O–C are somewhat variable because of packing interactions, but for the most part occur in the interval 142–

147°, including 1.²⁵ The square pyramidal stereochemistry observed here is now established as a general structural motif for molybdenum and tungsten complexes of the type $[\text{M}^{\text{IV}}(\text{QR})(\text{S}_2\text{C}_2\text{Me}_2)_2]^{1-}$ (Q = O, S, Se).^{1,24,25,31} In all such complexes, the chelate ring C–C and C–S bond lengths are consistent with an ene–dithiolate ligand electron distribution.

Synthesis and Structures of W(VI) Complexes. The diamagnetic monooxo W(VI) complexes 6–10 have been prepared by oxo transfer reaction 2. The green-brown or brown acetonitrile solution of a W(IV) complex undergoes an immediate color change to red-violet (6, 7, 10) or green-brown (8, 9)



upon the addition of 1.0–1.5 equiv of the *N*-oxide. Complexes 6 and 8 were isolated in substance; the remainder were generated in solution by oxo transfer reactions and identified by their absorption spectra. These complexes are also extremely dioxygen and water sensitive and must be handled under rigorously dry, anaerobic conditions. Complexes 6 and 8 in acetonitrile at ambient temperature slowly autoreduce over 1–2 days to $[\text{W}^{\text{V}}\text{O}(\text{S}_2\text{C}_2\text{Me}_2)_2]^{1-}$. (The corresponding molybdenum complexes are too unstable to isolate.³¹) Addition of 0.5 equiv of the *N*-oxide to a solution of 1 (δ 2.61) generates methyl NMR signals corresponding to a 50% conversion to 6 (δ 2.19). No other signals are observed, indicating that the conceivable reaction $\text{W}^{\text{IV}} + \text{W}^{\text{VI}}\text{O} \rightarrow \text{W}^{\text{V}}\text{O}-\text{W}^{\text{V}}$ is not favored. Related $\text{Mo}^{\text{V}}\text{O}-\text{Mo}^{\text{V}}$ complexes are readily formed, particularly from

(34) Craig, J. A.; Harlan, E. W.; Snyder, B. S.; Whitener, M. A.; Holm, R. H. *Inorg. Chem.* **1989**, *28*, 2082–2091.

(35) Doonan, C. J.; Slizys, D. A.; Young, C. G. *J. Am. Chem. Soc.* **1999**, *121*, 6430–6436.

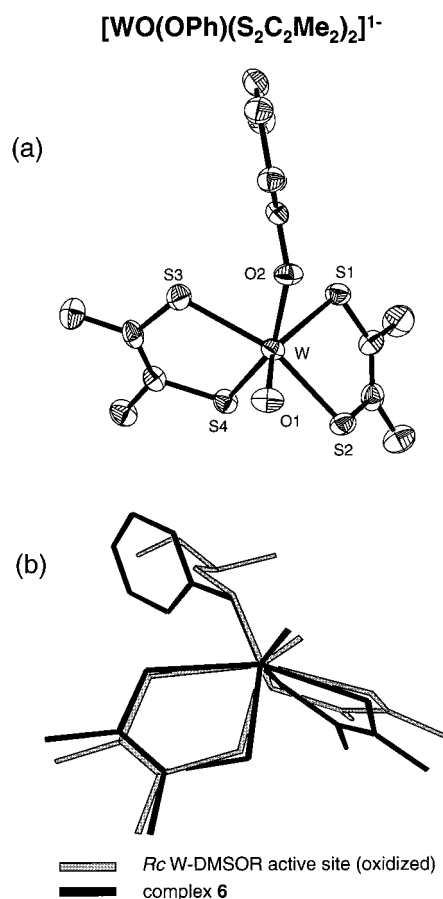


Figure 4. (a) Structure of monooxo complex **6** showing 50% probability ellipsoids and a partial atom labeling scheme. (b) Best-fit superposition of the cores of **6** and the active site of oxidized *Rf* W-DMSOR.²⁷ X-ray structural data for the enzyme in PDB format were obtained from the Brookhaven Protein Data Bank. The WS_4O_2 portions of **6** and the enzyme were fitted by using the subroutine OFIT of the SHELXS package.

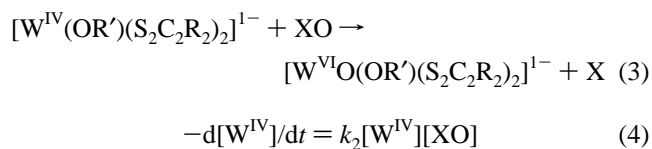
neutral $\text{Mo}^{\text{IV}}\text{O}$ and $\text{Mo}^{\text{VI}}\text{O}_2$ complexes,^{34,35} but thus far not from anionic bis(dithiolene) complexes with these oxometal groups.^{36,37} Using the strong oxo donor $\text{Ph}_2\text{Se}^{18}\text{O}$, we have established direct oxygen atom transfer to complex **1** with formation of $[\text{W}^{18}\text{O}(\text{OPh})(\text{S}_2\text{C}_2\text{Me}_2)_2]^{1-}$, demonstrated by IR spectroscopy. On this basis, we assume direct transfer from *N*-oxide and *S*-oxide substrates to this and other $\text{W}(\text{IV})$ complexes in the reactions that follow.

The structure of complex **6**, described briefly earlier,¹ is shown in Figure 4a; bond angles and distances are available in Table 3. The molecule exhibits an irregularly distorted octahedral stereochemistry with cis oxo (O1) and phenolate (O2) ligands. Atoms S(2,3) are mutually trans and cis to O(1,2). Distortions from an octahedral arrangement include a transoid $\text{S}2-\text{W}-\text{S}3$ angle of $153.49(5)^\circ$ and a dihedral angle between dithiolene rings of 99.8° . Values for octahedral/trigonal prismatic stereochemistry are $180^\circ/136^\circ$ and $90^\circ/120^\circ$. The trans influence of the oxo ligand is evident from the $\text{W}-\text{S}1$ bond distance of $2.492(1) \text{ \AA}$, 0.07 \AA longer than the mean of the three cis $\text{W}-\text{S}$ bonds. Complex **6** is isostructural with $[\text{WO}(\text{OSiBu}^t\text{R}_2)(\text{bdt})_2]^{1-}$ ($\text{R} = \text{Me}, \text{Ph}$),²⁰ $[\text{W}^{\text{VI}}\text{S}(\text{OSiBu}^t\text{Ph}_2)(\text{bdt})_2]^{1-}$,²⁰ and $[\text{MoO}(\text{OSiBu}^t\text{Ph}_2)(\text{bdt})_2]^{1-}$,²¹ a relationship that establishes the distorted cis-octahedral structural motif for molybdenum and

tungsten complexes of the type $[\text{M}^{\text{VI}}\text{Q}(\text{OR}')(\text{S}_2\text{C}_2\text{R}_2)_2]^{1-}$ ($\text{Q} = \text{O}, \text{S}$). This structure is chiral with four inequivalent methyl groups. In dichloromethane at room temperature, **6** exhibits one sharp methyl signal. The fluxional nature of this molecule is shown by the broadening of this signal as the temperature is decreased, until at 203 to 183 K two equally intense methyl signals appear at δ 1.9–2.4 (not shown). This observation is consistent with a species of mirror symmetry, such as a trigonal prismatic intermediate in the inversion of the complex by a trigonal twist mechanism that would equilibrate the four methyl groups.

The structure of **6** is compared in Figure 4b with that of *Rf* W-DMSOR determined with data up to 2.0 \AA resolution,²⁷ from which it is seen that the enzyme site in the six-coordinate model has the common feature of two cis oxygen atoms. The bond distances $\text{W}-\text{O} = 1.76$ and 1.89 \AA and $\text{W}-\text{S} = 2.44 \text{ \AA}$ from tungsten EXAFS correspond rather closely to those of **6** (Table 3). Analysis of positional deviations of the WS_4O_2 coordination spheres of both structures affords a weighted root-mean-square deviation of 0.39 \AA at this stage of resolution of the protein structure. While we cannot be precise about the structural differences, we can assert that **6** and the protein site have a similar overall stereochemistry with comparable bond lengths.

Kinetics of Oxo Transfer with *S*-Oxide and *N*-Oxide Substrates. With desoxo $\text{W}(\text{IV})$ and monooxo $\text{W}(\text{VI})$ complexes synthesized and structurally characterized, a kinetics study of reaction 3 with biological substrates $\text{XO} = \text{N}$ -oxide and *S*-oxide becomes feasible. Our first-generation Mo/W analogues $[\text{M}^{\text{IV}}(\text{OSiR}_3)(\text{bdt})_2]^{1-}$ are not suitable in this regard because of the slow to nil reaction rates with *S*-oxides at ambient temperature.^{20,21}



Reactivity with *S*-oxides was first examined by ^1H NMR. Addition of equimolar DMSO to a solution of complex **1** in acetonitrile resulted in no appreciable conversion to **6** over ~ 10 h. However, complete conversion to **6** in neat DMSO occurred within 4 h accompanied by development of the red-violet color and the upfield-shifted methyl signal (δ 2.19) characteristic of this complex. Thereafter, reaction 3 with $\text{XO} = \text{S}$ -oxide was examined under pseudo-first-order conditions and monitored by UV-visible absorbance changes. The time course of the system **1**/DMSO is depicted in Figure 5. The strong absorptions of **1** at 299 and 319 nm decrease in intensity with time and the features at 408, 514, and 637 nm increase. A tight isobestic point is observed at 337 nm. The final spectrum is identical with that of **6** measured separately. Because of the relatively slow reaction rate of this system ($k_2 = 3.9 \times 10^{-5} \text{ M}^{-1} \text{ s}^{-1}$ at 298 K), the only other *S*-oxide examined was TMSO, which under the same conditions reacts 23 times faster. In this and all other reaction systems with *S*-oxide substrates, k_{obs} is linearly dependent on $[\text{S-oxide}]_0$ even when the substrate is present in large excess. Saturation effects are not observed; Michaelis-Menten kinetics, as found in certain molybdenum-based oxo transfer systems, do not apply.^{36,38} All reactions adhere to the second-order rate law 4. Rate constants and activation parameters are collected in Table 4. The latter were evaluated from the Eyring equation; representative linear plots of $\ln(k/T)$ vs $1/T$ for three reactions are set out in Figure 6.

Several variables of the $\text{W}(\text{IV})$ reactant were examined with TMSO as the substrate. Replacement of the chelate ring methyl

(36) Das, S. K.; Chaudhury, P. K.; Biswas, D.; Sarkar, S. *J. Am. Chem. Soc.* **1994**, *116*, 9061–9070.

(37) Oku, H.; Ueyama, N.; Kondo, M.; Nakamura, A. *Inorg. Chem.* **1994**, *33*, 209–216.

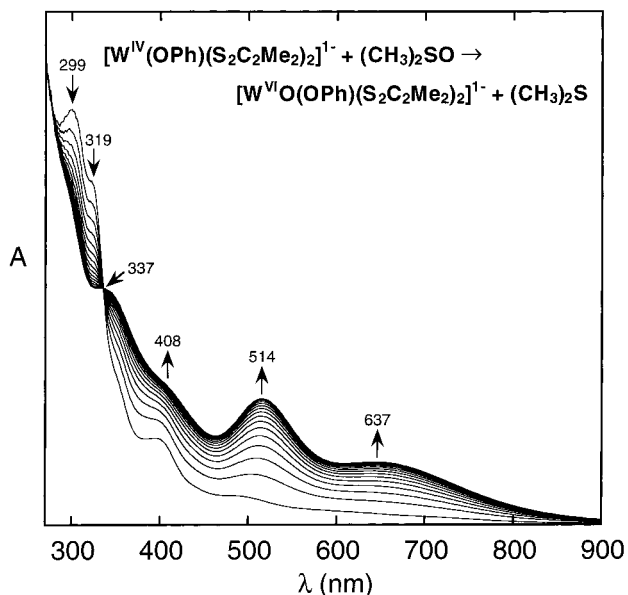


Figure 5. Absorption-spectral changes in the pseudo-first-order reaction **1** + Me₂SO → **6** + Me₂S in acetonitrile at 25 °C with [**1**]₀ = 1.2 mM and [Me₂SO]₀ = 2.3 M; spectra were recorded every 30 min. The final spectrum is identical with that of isolated complex **6**.

Table 4. Kinetics Data for Substrate Reduction by Oxo Transfer

R	XO	k_2 (M ⁻¹ s ⁻¹) ^a	ΔH^\ddagger (kcal/mol)	ΔS^\ddagger (eu)
Ph	Me ₂ SO	$3.9(4) \times 10^{-5}$	14.4(2)	-30(1)
Ph		$9.0(3) \times 10^{-4}$ ^b	11.6(4)	-33(1)
Ph	Ph ₂ AsO	3.2(1)	9.4(5)	-24(2)
Ph		0.34(1)	9.9(9)	-27(4)
<i>p</i> -C ₆ H ₄ CN		$3.5(1) \times 10^{-2}$	10.8(1)	-29(1)
<i>p</i> -C ₆ H ₄ Br		$4.2(1) \times 10^{-3}$	-	-
<i>p</i> -C ₆ H ₄ Me		$6.2(1) \times 10^{-4}$	-	-
<i>p</i> -C ₆ H ₄ OMe		$5.8(1) \times 10^{-4}$	-	-
<i>p</i> -C ₆ H ₄ NH ₂		$3.8(7) \times 10^{-4}$	15(1)	-24(4)
Pr ⁱ		4×10^{-6} ^c	-	-
Pr ⁱ	Me ₃ NO	0.93(5)	12(5)	-19(3)
Pr ⁱ		0.71(9)	11(6)	-23(5)

^a Acetonitrile solution, 298 K. ^b For the reaction of **2** with (CH₂)₄SO, $k_2 = 3.0(1) \times 10^{-3}$ M⁻¹ s⁻¹ at 298 K. ^c Measured in neat substrate at 298 K.

substituents ($\sigma_1 = -0.05$) with the less electron-releasing phenyl groups ($\sigma_1 = 0.10$) in complex **2** results $k_2(\mathbf{2})/k_2(\mathbf{1}) = 3.3$. Substitution of the terminal phenolate ligand in **6** with a range of para-substituted phenolate ligands in **5a–e** affords a ca. 90-fold range of rates, with the most electron-withdrawing substituent (X = CN, $\sigma_p = 0.69$) producing the largest rate

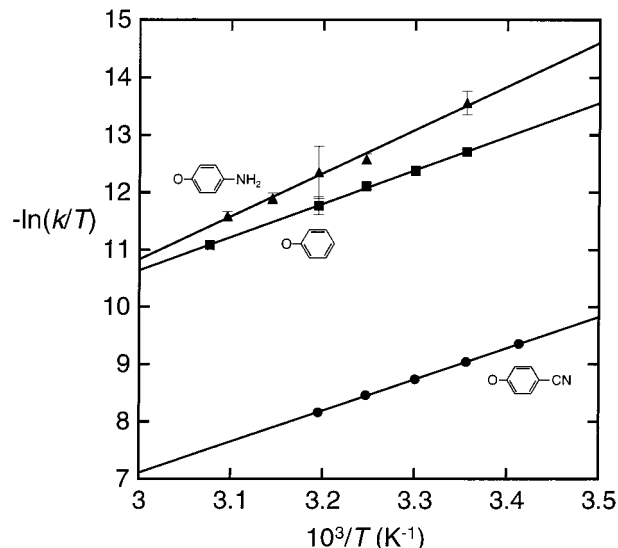


Figure 6. Eyring plots affording activation parameters for the reaction $[\text{W}^{\text{IV}}(\text{O}-p\text{-C}_6\text{H}_4\text{X})(\text{S}_2\text{C}_2\text{Me}_2)_2]^{1-} + \text{TMSO} \rightarrow [\text{W}^{\text{VI}}(\text{O}-p\text{-C}_6\text{H}_4\text{X})(\text{S}_2\text{C}_2\text{Me}_2)_2]^{1-} + \text{TMS}$ (X = CN, H, NH₂) in acetonitrile solutions.

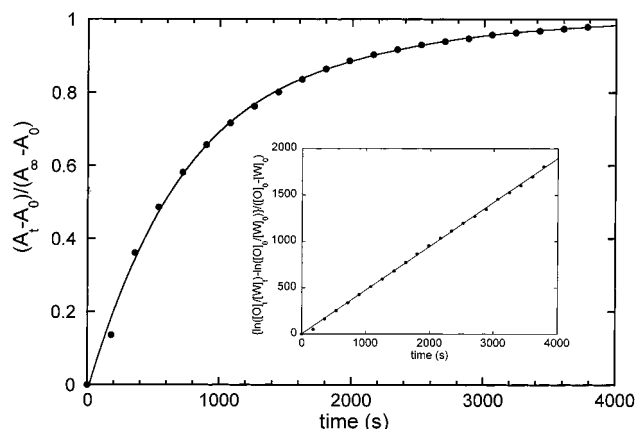


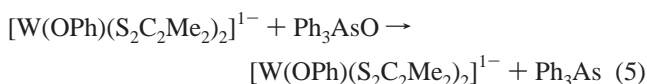
Figure 7. The time course of the reaction system with [**3**]₀ = 1.1 mM and [NMMO]₀ = 2.8 mM in acetonitrile at 298 K. The reaction was monitored at 487 nm. The value of $(A_t - A_0)/(A_\infty - A_0)$ is equal to the mole fraction of product **8**; the second-order rate constant k is directly obtained from the linear plot (inset).

enhancement. Replacement of phenolate with isopropoxide or 2-adamantyloxide, alkoxide ligands with a closer electronic resemblance to serinate, results in markedly diminished reactivity. Complexes **3** and **4** do not react with either DMSO or TMSO in ca. 1000-fold excess in acetonitrile at room temperature. At 373 K, these complexes are partially oxidized to **8** and **9** in very slow reactions; rate constants were not determined. Complex **3** is cleanly oxidized in neat TMSO (11.1 M) at 298 K. The time course of the reaction over 24 h is very similar to that in Figure 5 but is much slower; a tight isosbestic point occurs at 334 nm. The second-order rate constant $k_2 \approx 4 \times 10^{-6}$ M⁻¹ s⁻¹ is obtained. Although the comparison is inexact because of difference in solvent, the ratio $k_2(\mathbf{1})/k_2(\mathbf{3}) \approx 220$ emphasizes the appreciable reduction in rate upon replacement of phenolate with the more electron-rich isopropoxide ligand.

The relatively slow reactivity of complex **3** allowed kinetics measurements with Me₃NO and NMMO under second-order conditions. Spectrophotometric monitoring of the reaction system **3**/NMMO is shown in Figure 7. Adherence to second-order kinetics is apparent; the rate constant is obtained directly from the linear plot. Rate constants are ca. 10³–10⁵ larger than for the reactions of **1** and **3** with *S*-oxides. In addition to reaction

3, Me_3NO has been employed previously in the oxidations $[\text{W}^{\text{IV}}\text{O}(\text{bdt})_2]^{2-} \rightarrow [\text{W}^{\text{VI}}\text{O}_2(\text{bdt})_2]^{2-}$ ^{20,39} and $[\text{W}^{\text{IV}}(\text{OSiR}_3)(\text{bdt})_2]^{1-} \rightarrow [\text{W}^{\text{VI}}\text{O}(\text{OSiR}_3)(\text{bdt})_2]^{1-}$.²⁰

The reactions reported here contribute to the relatively small body of well-defined direct oxo transfer reactions mediated by tungsten.^{19,20,39–42} A majority of these reactions have been tabulated.^{19,40} Other than our initial report,¹ kinetics data for tungsten-mediated reactions have been confined to the systems $[\text{WO}(\text{bdt})_2]^{2-}/\text{Me}_3\text{NO}$, for which only k_{obs} at room temperature was reported,³⁹ and $[\text{WO}_2(\text{mnt})_2]^{2-}/(\text{MeO})_2\text{PhP}(\text{MeO})_3\text{P}$, for which rate constants and activation parameters were determined.¹⁹ Our thermodynamic oxo transfer reaction scale is based on ΔG or ΔH values for the reaction couples $\text{X}_{(\text{g})} + \frac{1}{2}\text{O}_{2(\text{g})} \rightarrow \text{XO}_{(\text{g})}$. For the couples involving Me_3NO , Me_2SO , and Ph_3AsO , $\Delta H = -2$, -27 , and -43 kcal/mol, respectively.⁴³ The spontaneous occurrence of reaction 5 demonstrates that complex **1** is a stronger oxo acceptor than Ph_3As , and that for the couple **1** + $\frac{1}{2}\text{O}_{2(\text{g})} \rightarrow \mathbf{6}$, $\Delta H < -43$ kcal/mol. This marks **1** as a relatively strong oxo acceptor, comparable to, e.g., MoCl_4 (ΔH



$= -41$ kcal/mol). In an attempt to set a lower limit of **1** on the oxo transfer scale, further reactions were investigated. No reaction was observed between **1** and 100 equiv of Ph_3PO ($\Delta H = -74$ kcal/mol) at 50 °C for 1 day. Under similar conditions with Ph_3P and **6**, the reverse reaction of substrate oxidation did not occur over a 10 h period. With 200–700 equiv of the more basic Et_3P , a slow reaction at room temperature proceeded to form a yellow solution, the absorption spectrum of which suggests that the product is the bis(phosphine) complex $[\text{W}(\text{PEt}_3)_2(\text{S}_2\text{C}_2\text{Me}_2)_2]$, analogous to $[\text{W}(\text{P}(\text{OEt})_3)_2(\text{bdt})_2]$ and $[\text{Mo}(\text{PMePh}_2)_2(\text{bdt})_2]$, which have been isolated.^{20,21} While the lack of a reaction cannot establish a lower limit, the implication is that complex **1** is a less strong oxo acceptor than Ph_3P or WCl_4 ($\Delta H = -67$ kcal/mol).

Mechanistic Considerations. The most thorough experimental analysis of the mechanism of a molybdenum- or tungsten-mediated oxo transfer is that of $[\text{Mo}^{\text{IV}}\text{O}(\text{Bu}^t\text{L-NS})_2]$ with *N*-oxides, *S*-oxides, and Ph_3AsO .⁴⁴ Although the minimal reaction in question, $\text{Mo}^{\text{IV}}\text{O} + \text{XO} \rightarrow \text{Mo}^{\text{VI}}\text{O}_2 + \text{X}$, is not that examined here (nor a known enzymatic process), certain considerations are pertinent as in the corresponding bis-(dithiolene)molybdenum systems.³¹ Reference is made to the rate constants and activation parameters in Table 4. All reactions are second order with $|\Delta H| > |T\Delta S|$ and large negative entropies of activation for *N*-oxides (-19 to -27 eu), *S*-oxides (-24 to -33 eu), and Ph_3AsO (-24 eu), which indicate associative transition states. For the most part $T\Delta S^\ddagger$ is approximately constant, such that ΔH^\ddagger is 55–68% of ΔG^\ddagger . We look into the nature of the transition state by examining the effects of ligand and substrate variation on reaction rates which are expected to influence primarily activation enthalpies. Ligand effects are considered first.

The relative rates $k_2(\mathbf{2})/k_2(\mathbf{1}) = 3.3$ and $k_2(\mathbf{3})/k_2(\mathbf{1}) \approx 0.0045$ with TMSO imply that substrate binding, i.e., $\text{W}\cdots\text{OX}$ bond

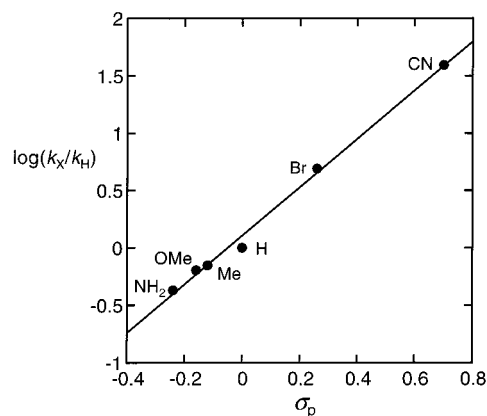


Figure 8. Hammett plot of $\log(k_X/k_H)$ vs σ_p for the reaction series **1** and **5a–e** + TMSO \rightarrow **6** and **10a–e** + TMS in acetonitrile at 298 K.

Table 5. Properties of Substrates XO (the quantities GB and PA refer to the reaction $\text{M}_{(\text{g})} + \text{H}^+_{(\text{g})} = \text{MH}^+_{(\text{g})}$ at temperature T)

XO	$\Delta H_{\text{X/XO}}^a$	$D_{\text{X-O}}^a$	GB ^b	PA ^c	$\text{p}K_{\text{a}}(\text{BH}^+)$ (medium)
Me_3NO	-2	61 ^d	227.9	235.0	4.65 ^e (aq)
	-11	71 ^f			18.68 ^g (acetonitrile)
NO	-13	72 ^h	213.4	220.7	0.79 ⁱ (aq)
					10.04 ^j (acetonitrile)
Me_2SO	-27	87	204.0	211.4	-1.80 ^k (aq)
SO	-26	86 ^l	N/A	N/A	-1.34 ^l (aq)
Ph_3AsO	-43	103	209.5	216.6	0.99 ^m (aq)
Ph_3PO	-74	133	209.5	216.6	-2.10 ^m (aq)

^a $D = -\Delta H_{\text{X/XO}} + \Delta_f H^\circ_{\text{m}}(\text{O}_{(\text{g})})$; ref 43. ^b Gas basicity, $\text{GB}(\text{M}) = -\Delta G^\circ$; ref 46. ^c Proton affinity, $\text{PA}(\text{M}) = -\Delta H^\circ = \Delta_f H^\circ(\text{M}) + \Delta_f H^\circ(\text{H}^+) - \Delta_f H^\circ(\text{MH}^+)$; ref 46. ^d Reference 47. ^e Reference 48. ^f Reference 49. ^g Reference 50. ^h Reference 51. ⁱ Reference 52. ^j Reference 53. ^k Reference 54. ^l Reference 55. ^m Reference 56.

making, is significant in the transition state. The first ratio suggests that reducing the basicity of the dithiolene by substituting methyl with phenyl leads to a small rate enhancement. The second ratio indicates that substitution of a more basic oxygen ligand, Pr^{O^-} for PhO^- , without an increase in steric hindrance at the metal site significantly, retards the reaction rate. Thereafter, in reactions with TMSO the electronic effect of the axial ligand was examined by using the set of complexes **1** and **5a–e**, in which the para-substituent X of the axial phenolate ligands $p\text{-XC}_6\text{H}_4\text{O}^-$ was varied without introducing significant steric differences. The reaction products were shown by spectral comparison with authentic samples to be **6** and **10a–e** (Figure 2). As shown in Figure 8, the rate constants fit the Hammett equation $\log(k_X/k_H) = \rho\sigma_p$. The positive slope $\rho = 2.1$ shows that electron-withdrawing groups accelerate the rate, with limiting ratios being $k_{\text{CN}}/k_{\text{H}} = 39$ and $k_{\text{H}}/k_{\text{NH}_2} = 2.4$. The effects are not large but the trend is clear from these and the preceding rate constant ratios: rates increase in a manner qualitatively consistent with diminution of electron density at the tungsten center.

Assembled in Table 5 are certain thermodynamic properties of substrates XO, including $\Delta H_{\text{X/XO}}$ in the thermodynamic reactivity scale, bond dissociation energies D , gas basicities GB,

(38) Berg, J. M.; Holm, R. H. *J. Am. Chem. Soc.* **1985**, *107*, 925–932.

(39) Ueyama, N.; Oku, H.; Nakamura, A. *J. Am. Chem. Soc.* **1992**, *114*, 7310–7311.

(40) Holm, R. H. *Chem. Rev.* **1987**, *87*, 1401–1449.

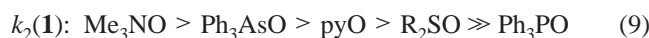
(41) Yu, S.-B.; Holm, R. H. *Inorg. Chem.* **1989**, *28*, 4385–4391.

(42) Lee, S.; Staley, D. L.; Rheingold, A. L.; Cooper, N. J. *Inorg. Chem.* **1990**, *29*, 4391–4396.

(43) Holm, R. H.; Donahue, J. P. *Polyhedron* **1993**, *12*, 571–589.

(44) Schultz, B. E.; Holm, R. H. *Inorg. Chem.* **1993**, *32*, 4244–4248.

proton affinities PA, and solution basicity constants.^{43,46–56} We take the faster reaction of TMSO than DMSO with complex **1**, expressed by $k_2^{\text{TMSO}}/k_2^{\text{DMSO}} = 23$, to reflect a small steric effect owing to the ring structure of TMSO (and possibly a slightly higher basicity), which should facilitate binding to the tungsten center. The D values of the two substrates are essentially the same and aqueous basicities are quite similar. Properties are conveniently considered in terms of the series 6–8. The bond energy order P–O > As–O > S–O > N–O in series 6 is clear-cut and is based mainly on thermochemical data. In the proton affinity series 7, the two N -oxides are the most basic. The order is unclear for Ph_3PO and Ph_3AsO whose PA values are quoted from “bracketing” experiments intended to define a limited range of values for a series of bases.⁵⁷ Aqueous protonation constants for the reaction $\text{XO} + \text{H}^+ \rightleftharpoons \text{XOH}^+$ were not all measured by the same technique. Examination of all available data indicates that the order of series 8 is appropriate. These series may be compared to the rate constant orders 9 and 10. In series 9, Me_3NO is placed at the fast end because its reaction with **1** under the same conditions for Ph_3AsO is too rapid to measure by the spectrophotometric method used. Ph_3PO is placed at the slow end because of the lack of reaction between **1** and this compound in excess. The order in series 10 is experimental.



The inverse of series 6 would be expected to apply to k_2 values if substrate X–O bond weakening dominated the transition state. However, Ph_3AsO has a much higher reactivity than would be expected on this basis. Series 7 or 8 is pertinent if proton affinities in the gas or aqueous phase reflect the substrate binding affinities toward W(IV) centers. Possible mechanistic pathways are summarized in Figure 9. If $\Delta H^\ddagger_1 > \Delta H^\ddagger_2$, the higher transition state is early and is dominated by $\text{W}\cdots\text{OX}$ bond making with little X–O bond weakening. If $\Delta H^\ddagger_2 > \Delta H^\ddagger_1$, the higher transition state is late and involves considerable X–O bond weakening or dissociation and incipient and concomitant oxygen atom transfer and oxidation of the initial W(IV) center. Either situation involves an extent of structural rearrangement as the five-coordinate complex acquires

(45) Laughlin, L. J.; Young, C. G. *Inorg. Chem.* **1996**, *35*, 1050–1058.
 (46) Hunter, E. P.; Lias, S. G. *J. Phys. Chem. Ref. Data* **1998**, *27*, 413–656 and references therein.

(47) Acree, W. E., Jr.; Tucker, S. A.; Ribeiro da Silva, M. D. M. C.; Matos, A. R.; Gonçalves, J. M.; Ribeiro da Silva, M. A. V. *J. Chem. Thermodyn.* **1995**, *27*, 391–398.

(48) Nylén, P. *Z. Anorg. Allg. Chem.* **1941**, *246*, 227–330.
 (49) Haaland, A.; Thomassen, H. *J. Mol. Struct.* **1991**, *263*, 299–310.
 (50) Chmurzyński, L.; Pawlak, Z. *J. Chem. Thermodyn.* **1998**, *30*, 27–35.

(51) Shaofeng, L.; Pilcher, G. *J. Chem. Thermodyn.* **1988**, *20*, 463–465.

(52) (a) Jaffé, H.; Doak, G. O. *J. Am. Chem. Soc.* **1955**, *77*, 4441–4444. (b) Kubota, T. *J. Am. Chem. Soc.* **1965**, *87*, 458–468.

(53) Landini, D.; Modena, G.; Scorrano, G.; Taddei, F. *J. Am. Chem. Soc.* **1969**, *91*, 6703–6707.

(54) Jenks, W. S.; Matsunaga, N.; Gordon, M. *J. Org. Chem.* **1996**, *61*, 1275–1283.

(55) Curci, R.; Furia, F.; Levi, A.; Lucchini, V.; Scorrano, G. *J. Chem. Soc. Perkin Trans. 2* **1975**, 341–344.

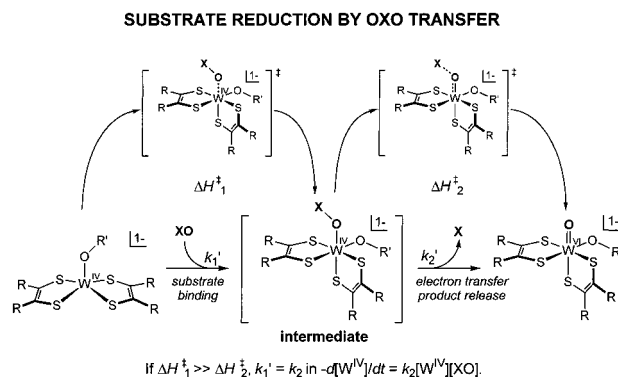
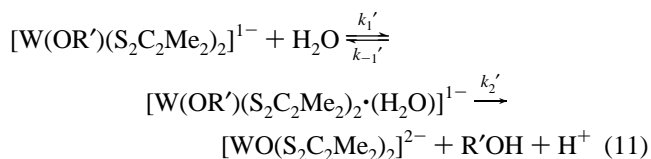


Figure 9. Mechanistic pathways for oxygen atom transfer from substrate XO to $[\text{W}^{\text{IV}}(\text{OR}')(\text{S}_2\text{C}_2\text{R}_2)_2]^{1-}$. If $\Delta H^\ddagger_1 > \Delta H^\ddagger_2$, the transition state is early and is dominated by $\text{W}\cdots\text{OX}$ bond-making with little X–O bond-weakening. The opposite situation leads to a late transition state with substantial X–O bond weakening and concomitant atom transfer and oxidation of initial W(IV) .

another ligand. The indicated intermediate and by the Hammond postulate the two transition states are expected to have structures approaching that of product complex **6**.⁵⁸ The observation that series 9 parallels series 8 suggests an early transition state involving considerable $\text{W}^{\text{IV}}\cdots\text{OX}$ bond making.

Hydrolysis Reactions. As noted earlier, the W(IV,VI) complexes isolated in this work are highly sensitive to water. When the green-brown and brown acetonitrile solutions of **1** and **3**, respectively, are treated with 1000–20000 equiv of water, they slowly turn to the characteristic orange-brown color of **11**. The rates of the hydrolysis of complexes **1** and **3** have been determined at room temperature. Spectrophotometric monitoring of the reactions reveals well-defined isosbestic points at 632 (**1** → **11**) and 624 nm (**3** → **11**). As shown in Figure 10, pseudo-first-order plots of k_{obs} vs $[\text{H}_2\text{O}]$ are nonlinear, showing saturation kinetics at high substrate concentrations. The data are well-fitted to Michaelis–Menten kinetics reaction 11; double reciprocal plots generate straight lines which afford first-order rate constant k_2' and K_M . Data are contained in Table 6. The reaction involves a preequilibrium between **1** or **3** and an aqua-bound species followed by release of PhOH or PrOH in the rate-determining step. The rate constant $k_2' = 7.8 \times 10^{-4} \text{ s}^{-1}$ for the hydrolysis of **1** indicates a rather slow reaction. The value $k_2'/K_M = 1.7 \times 10^{-4} \text{ M}^{-1} \text{ s}^{-1}$ is comparable to rate constants for S -oxides (Table 4), and emphasizes the need for



$$k_{\text{obs}} = \frac{k_2'[\text{H}_2\text{O}]}{K_M + [\text{H}_2\text{O}]}, \quad K_M = \frac{k_{-1}' + k_2'}{k_1'}$$

dry conditions when examining the reduction of these substrates. The rate constant for **3** is nearly the same as that for **1**. The substantial primary isotope effects $k_2^{\text{H}}/k_2^{\text{D}} = 3.1$ and 5.6 reflect

(56) Klofutar, C.; Krašovec, F.; Kušar, M. *Croat. Chim. Acta* **1968**, *40*, 23–28 and references therein.

(57) Tran, V. T.; Munson, B. *Org. Mass Spectrom.* **1986**, *21*, 41–46.

(58) A somewhat related discussion has been presented for the reaction of oxo donors with carbonyl ligands: Kelly, A. M.; Rosini, G. P.; Goldman, A. S. *J. Am. Chem. Soc.* **1997**, *119*, 6115–6125.

(59) Lorber, C.; Plutino, M. R.; Elding, L. I.; Nordlander, E. *J. Chem. Soc., Dalton Trans.* **1997**, 3997–4003.

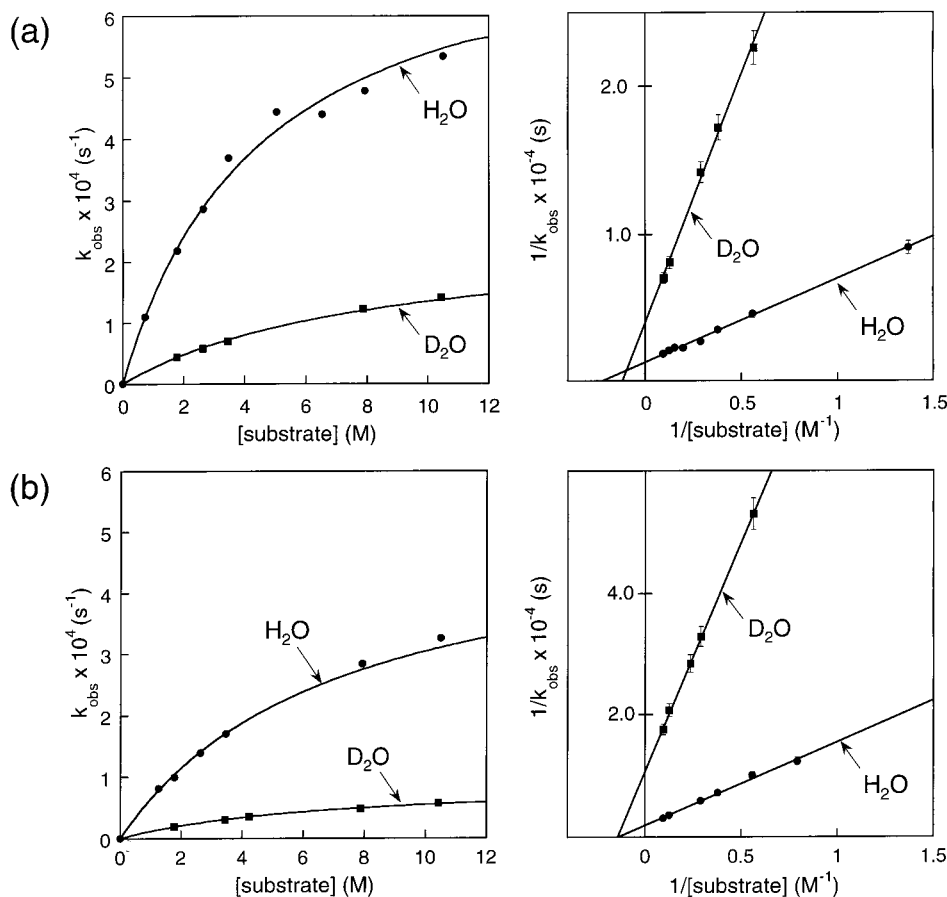
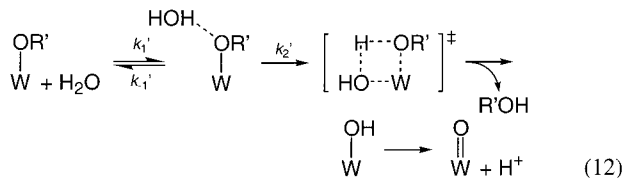


Figure 10. Dependence of the observed rate constants on substrate concentration for hydrolysis reaction 11 involving (a) **1** and (b) **3**.

Table 6. Kinetics Data of the Hydrolysis of Complexes **1** and **3** at 298 K

complex	substrate	k_2' (s^{-1})	K_M (M)	k_2'/K_M ($M^{-1} s^{-1}$)	k_2^{H}/k_2^{D}
[W(OPh)(S ₂ C ₂ Me ₂) ₂] ¹⁻ (1)	H ₂ O	$7.8(2) \times 10^{-4}$	4.5	1.7×10^{-4}	3.1
	D ₂ O	$2.5(1) \times 10^{-4}$	8.4	3.0×10^{-5}	
[W(OPr ^t)(S ₂ C ₂ Me ₂) ₂] ¹⁻ (3)	H ₂ O	$5.2(1) \times 10^{-4}$	7.1	7.3×10^{-5}	5.6
	D ₂ O	$9.3(1) \times 10^{-5}$	7.0	1.3×10^{-5}	

proton transfer in the transition state. In the proposed reaction 12, water may first associate with the complex by hydrogen bonding to the axial ligand, followed by formation of a concerted transition state with W...OH₂ and H...OR' bond making and W-OR' bond weakening. Thereafter, proton transfer is completed, R'OH dissociates, and the W^{IV}=O bond is developed. The larger isotope effect is associated with the more basic axial ligand. The rate comparison $k_2^{Mo}/(k_2'/K_M)^W \approx 70$, involving **1** and [Mo(OPh)(S₂C₂Me₂)₂]¹⁻,^{31,60} is consistent with the expected stronger W-OR' bond.



Comparative Molybdenum and Tungsten Reactivities.

Summarized in Table 1 are relative reactivities of three types of molybdenum/tungsten isoenzymes. Structural information is available only for *Rc* Mo- and W-DMSOR. A seemingly reasonable but unproven assumption is that catalytic sites at the same oxidation level in these isoenzymes have the same structure. As demonstrated with bis(dithiolenes)^{1,19–25,37,61} and

other classes of compounds, isoelectronic molybdenum and tungsten molecules are isostructural and essentially isometric. We have already noted that the active site formulation [W^{VI}O(O·Ser)(S₂pd)₂] is consistent with crystallographic and EXAFS results²⁷ and the structure is related to **6** (Figure 4). DMSORs reduce both DMSO and Me₃NO,^{62,63} whereas TMAORs thus far reduce only *N*-oxides at a measurable rate.²⁶ Although the small database renders any inquiry preliminary, we have become interested in whether relative rates of isoenzymes are intrinsic to the metal. To proceed, we examine Table 7, which contains kinetic data for oxo transfer by pairs of isoelectronic molybdenum and tungsten complexes. Upon comparison of data for isoenzymes and synthetic complexes, a parallel behavior emerges: oxo transfer from substrate to metal is faster with tungsten,⁶⁴ and oxo transfer to substrate from metal is faster with molybdenum. Oxo transfer from and to substrate

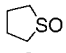
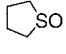
(60) Unlike **1**, [Mo(OPh)(S₂C₂Me₂)₂]¹⁻ does not exhibit saturation behavior over the water concentration range that afforded measurable rates by the spectrophotometric method used. Consequently, second-order rate constants are compared.

(61) Das, S. K.; Biswas, D.; Maiti, R.; Sarkar, S. *J. Am. Chem. Soc.* **1996**, *118*, 1387–1397.

(62) Adams, B.; Smith, A. T.; Bailey, S.; McEwan, A. G.; Bray, R. C. *Biochemistry* **1999**, *38*, 8501–8511.

(63) Simala-Grant, J. L.; Weiner, J. H. *Eur. J. Biochem.* **1998**, *251*, 510–515 and references therein.

Table 7. Comparative Kinetics Data of M = Mo and W Oxo Transfer at 298 K

reaction	substrate X or XO	k_2 ($M^{-1}s^{-1}$)		W/Mo reactivity ratio	ref
		M = Mo	M = W		
M(VI) → M(IV)					
$[MO_2(mnt)_2]^{2-} + X \rightarrow [MO(mnt)_2]^{2-} + XO$	(MeO) ₂ PhP	0.45(2)	$4.5(2) \times 10^{-4}$	0.001	19
	(MeO) ₃ P	$2.5(1) \times 10^{-2}$	9.7×10^{-6}	0.0004	19
	(EtO) ₂ MeP	1.1	3.4×10^{-3}	0.003	19
	Na ⁺ HSO ₃ ⁻	87 ^a	no reaction	-	36, 59
M(IV) → M(VI)					
$[MO(bdt)_2]^{2-} + XO \rightarrow [MO_2(bdt)_2]^{2-} + X$	Me ₃ NO	2.0×10^{-3}	5.0×10^{-3}	2.5	39
$[M(OPh)(S_2C_2Me_2)_2]^{1-} + XO \rightarrow$ $[MO(OPh)(S_2C_2Me_2)_2]^{1-} + X$	Me ₂ SO	1.3×10^{-6}	$3.9(4) \times 10^{-5}$	30	1, b
		$1.5(2) \times 10^{-4}$	$9.0(3) \times 10^{-4}$	6	1, b
$[M(OPh)(S_2C_2Ph_2)_2]^{1-} + XO \rightarrow$ $[MO(OPh)(S_2C_2Ph_2)_2]^{1-} + X$		$3.4(2) \times 10^{-4}$	$3.0(1) \times 10^{-3}$	8.8	31, b

^a k_2'/K_M from Michaelis–Menten kinetics performed in MeCN/H₂O = 1/1 (v/v) at 20 °C. ^b This work.

leads to metal oxidation and reduction, respectively. Elsewhere we have enumerated properties that may contribute to differential reaction rates of molybdenum/tungsten pairs,¹⁹ among which are redox potentials. It is always true that $E_{Mo} > E_W$, a behavior illustrated by $E_{Mo} - E_W = 0.29, 0.20$ V for the reversible redox couples $[MO(S_2C_2Me_2)_2]^{2-/-1-}$.^{22,24} While it is conceivable that parallel reactivity ratios, in the sense of $k^W/k^{Mo} > 1$ or < 1 , in the two tables is coincidental, the reactivity ratios could also reflect the inherent oxidizability or reducibility of the metal in a consistent manner. Given that there is a “metal effect” on rates, the preceding concept of the transition state requires alteration. Following intermediate formation, the system may pass through a highly concerted transition state with X–O bond-weakening and W–O bond-making with incipient atom transfer and metal oxidation. Further consideration of the nature of the transition state may be assisted by theoretical studies of the reaction coordinate, as has been done for the reactions $Mo^{VI}O_2 + R_3P \rightarrow Mo^{IV}O + R_3PO$ (R = H, Me).⁶⁵

Summary. This investigation presents the synthesis and structures of potential or real analogues of the active sites of tungsten-containing DMSOR, TMAOR, and possibly FMDH (iso)enzymes, and the first extensive kinetics study of substrate reduction via oxo transfer mediated by bis(dithiolene)tungsten complexes. The following are the principal results and conclusions of this research.

(1) The desoxo complexes $[W^{IV}(OR')(S_2C_2R_2)_2]^{1-}$ (R = Me, Ph) are readily prepared by carbonyl substitution reactions of $[W(CO)_2(S_2C_2R_2)_2]$, further emphasizing the utility of the dicarbonyls as precursors to variously substituted bis(dithiolene)W(IV) species. These complexes readily react with Me₃NO to afford the monooxo complexes $[W^{VI}O(OR')(S_2C_2R_2)_2]^{1-}$, two of which ($[W^{VI}O(OR')(S_2C_2Me_2)_2]^{1-}$, R = Ph, Prⁱ) have been isolated.

(2) The structures of the desoxo W(IV) complexes are square pyramidal with the metal atom 0.74–0.78 Å above the S₄ plane

(64) We have observed one possible deviation from this behavior. In the reduction of TMSO by **3** (Table 4) and $[Mo(OPr^i)(S_2C_2Me_2)_2]^{1-}$ in neat TMSO, $k_2^W/k_2^{Mo} \sim 0.8$. Given the errors in the rate constants of these extremely slow reactions, we conclude that the rates are essentially the same.

(65) (a) Pietsch, M. A.; Hall, M. B. *Inorg. Chem.* **1996**, *35*, 1273–1278. (b) Thomson, L. M.; Hall, M. B. *J. Am. Chem. Soc.* Submitted for publication.

toward the axial ligand and dithiolene ligands disposed at dihedral angles of 126–130°. The complex $[W^{VI}O(OPh)(S_2C_2Me_2)_2]^{1-}$ adopts a distorted cis-octahedral structure and is fluxional in solution. These structures are taken as those of oxidized and reduced protein-bound sites when unconstrained by the protein. Comparison with the structure of *Rc* W-DMSOR reveals similarities in overall stereochemistry and W–O and W–S bond lengths.

(3) The complexes $[W^{IV}(OR')(S_2C_2Me_2)_2]^{1-}$ (R' = Ph, *p*-XC₆H₄, Prⁱ) engage in direct oxo transfer reactions with *N*-, *As*-, *S*-, and *Se*-oxides to afford $[W^{VI}O(OR')(S_2C_2Me_2)_2]^{1-}$ in clean transformations. Direct atom transfer was demonstrated with Ph₂Se¹⁸O.

(4) The reactions in (3) are second order and proceed through associative transition states ($\Delta S^\ddagger = -19$ to -33 eu). For $[W^{IV}(OPh)(S_2C_2Me_2)_2]^{1-}$, rates or rate constants k_2 follow the substrate order Me₃NO > Ph₃AsO > pyO > R₂SO ≫ Ph₃PO. The W(IV) complexes are intrinsically capable of reducing both *N*-oxides and *S*-oxides, although at very different rates. This behavior contrasts with the apparent lack of reduction of *S*-oxides by TMAORs, and suggests possible enzymic reduction of *S*-oxides but at very slow rates relative to *N*-oxide reduction.

(5) Comparison of relative reactivities of Mo/W isoenzymes and pairs of isostructural Mo/W complexes at parity of ligation reveals that oxo transfer from substrate to metal is faster with tungsten and to substrate from metal is faster with molybdenum. These results demonstrate a kinetic metal effect in direct oxo transfer reactions for analogue complexes and for isoenzymes provided the catalytic sites are isostructural.

(6) The results in (4) and (5) and the influence on rates by variation of axial oxygen ligands leads to the tentative conception of a highly concerted transition state involving primarily W–OX bond-making and incipient atom transfer and metal oxidation.

(7) The W(IV,VI) complexes reported here are highly water sensitive. The kinetics of hydrolysis of $[W^{IV}(OR')(S_2C_2Me_2)_2]^{1-}$ (R' = Ph, Prⁱ) exhibit saturation kinetics with $k_2' \sim 10^{-3} s^{-1}$ and primary isotope effects indicative of proton transfer in the transition state.

Last, we reemphasize that the databases of comparative Mo/W kinetics used in (5) are not extensive, the similarities or

differences in enzyme active site structures are largely unknown, rate-limiting features of catalytic cycles have not been defined, and reactivity differences are relatively small for substrate reduction reactions. It will be most interesting to learn if further data sustain a parallel reactivity between isoenzymes and analogue complexes. Current research is directed at clarifying (6) and investigating other reactions of tungstoenzymes.

Acknowledgment. This research was supported by NSF Grant CHE-98-76457. We thank B. S. Lim for useful discussions

and Professors H. Schindelin and M. B. Hall for access to refs 7 and 65b, respectively, prior to publication.

Supporting Information Available: X-ray crystallographic data for structure determination of the five compounds listed in Table 2 (PDF). This material is available free of charge via the Internet at <http://pubs.acs.org>.

JA0036559